An interpretation for the components of $2p_{3/2}$ core level x-ray photoelectron spectra of the cations in some inverse spinel oxides

OPEN ACCESS
IOP Publishing
Journal of Physics: Condensed Matter
J. Phys.: Condens. Matter **36** (2024) 285001 (10pp)
https://doi.org/10.1088/1361-648X/ad3271

An interpretation for the components of $2p_{3/2}$ core level x-ray photoelectron spectra of the cations in some inverse spinel oxides

Arjun Subedi[1,*], Detian Yang[1], Wai Kiat Chin[1], Binny Tamang[2], Sushrisangita Sahoo[3], Paul Yancey[4], Rifat Mahbub[5], Jeffrey Shield[5], Rebecca Y Lai[2], Xiaoshan Xu[1], Peter A Dowben[1] and Vijaya Rangari[3]

[1] Department of Physics and Astronomy, Theodore Jorgensen Hall, University of Nebraska-Lincoln, 855 North 16th Street, Lincoln, NE 68588-0299, United States of America
[2] Department of Chemistry, Hamilton Hall, University of Nebraska-Lincoln, Lincoln, NE 68588-0304, United States of America
[3] Department of Material Science and Engineering, Tuskegee University, Tuskegee, AL 36088, United States of America
[4] Department of Mechanical Engineering, Materials Processing Laboratory, Tuskegee University, Tuskegee, AL 36088, United States of America
[5] Department of Mechanical and Materials Engineering, 339 Nebraska Hall, University of Nebraska, Lincoln, NE 68588-0526, United States of America

E-mail: arjun.subedi@huskers.unl.edu

Received 26 January 2024, revised 29 February 2024
Accepted for publication 11 March 2024
Published 12 April 2024

Abstract

In an effort to reconcile the various interpretations for the cation components of the $2p_{3/2}$ observed in x-ray photoelectron spectroscopy (XPS) of several spinel oxide materials, the XPS spectra of both spinel alloy nanoparticles and crystalline thin films are compared. We observed that different components of the $2p_{3/2}$ core level XPS spectra, of these inverse spinel thin films, are distinctly surface and bulk weighted, indicating surface-to-bulk core level shifts in the binding energies. Surface-to-bulk core level shifts in binding energies of Ni and Fe $2p_{3/2}$ core levels of $NiFe_2O_4$ thin film are observed in angle-resolved XPS. The ratio between surface-weighted components and bulk-weighted components of the Ni and Fe core levels shows appreciable dependency on photoemission angle, with respect to surface normal. XPS showed that the ferrite nanoparticles $Ni_xCo_{1-x}Fe_2O_4$ ($x = 0.2, 0.5, 0.8, 1$) resemble the surface of the $NiFe_2O_4$ thin film. Surface-to-bulk core level shifts are also observed in $CoFe_2O_4$ and $NiCo_2O_4$ thin films but not as significantly as in $NiFe_2O_4$ thin film. Estimates of surface stoichiometry of some spinel oxide nanoparticles and thin films suggested that the apportionment between cationic species present could be farther from expectations for thin films as compared to what is seen with nanoparticles.

* Author to whom any correspondence should be addressed.

Supplementary material for this article is available online

Keywords: spinel oxides, x-ray photoelectron spectroscopy, surface-to-bulk core level shift

1. Introduction

Spinel oxide thin films and nanoparticles are among some of the most extensively studied oxide systems using various characterization techniques for several electric and magnetic properties [1–5]. One of the frequently used characterization techniques for such systems is x-ray photoelectron spectroscopy (XPS) [6–32] which is performed mainly for the study of surface chemistry and surface electronic properties. Although there have been numerous XPS of several inverse spinel oxide materials, there has been no consensus on the interpretation for the cation components of the $2p_{3/2}$ XPS spectra for the inverse spinel oxides of type AB_2O_4 (examples $NiCo_2O_4$, $CoFe_2O_4$, $NiFe_2O_4$, etc). A typical XPS spectrum of Ni $2p_{3/2}$ core level in $NiCo_2O_4$, one of the inverse spinel oxides, is shown in the figure 1. The spectrum contains three components: P_1, P_2, and S.

Although the feature labeled S (in figure 1) is consistently identified as the commonly observed core level satellite feature, in the XPS spectra of many transition metal oxides, there has been various interpretations of two component peaks of type P_1 and P_2 as shown in figure 1. Apparently, for the inverse spinel oxide systems of type AB_2O_4, there appear to be four interpretations that are frequently mentioned in the literature, when P_1 and P_2 type component XPS peaks (as shown in figure 1) of the A-type and B-type elements are assigned. One explanation put forth is that P_1 is the $+2$ cationic state and P_2 is the $+3$ cationic state of both A-type and B-type elements [6–8]. Alternatively, P_1 is assigned to the $+3$ cationic state and P_2 is the $+2$ cationic state of both A-type and B-type elements [9–12]. Then there is the assignment that P_1 is the $+2$ cationic state and P_2 is the $+3$ cationic state for one of the elements between A and B, but for the other element P_1 component corresponds to the $+3$ state while the P_2 component corresponds to the $+2$ state [13–20]. By far the most common explanation that has been put forward has been that the P_1 XPS component is a result of the metal cation occupancy in the octahedral site while the P_2 XPS component is the result of occupancy of the metal cation in the tetrahedral site, both components with the same cationic states [13, 21–32]. Clearly this represents a situation where there is no general agreement on the assignment of the component peaks seen in the XPS spectra of the transition metal constituents.

Complicating an assessment that leads to an ambiguous assignment of the different core level binding energy features seen in the XPS $2p$ core level spectra is that photoemission is a final state spectroscopy and contains contributions from both initial state and final state effects [33–38]. If we just consider initial state effects, which mainly include the effects of chemical bonding, charge transfer and neighbor interactions on binding energy before the photoemission event, binding energies for different cationic states should have the order of $A^0 < A^{1+} < A^{2+} < A^{3+}$…. [34, 35]. This would favor an assignment where P_1 is the $+2$ cationic state and P_2 is the $+3$ cationic state, in the transition metal $2p$ core level XPS spectra. In the photoemission, however, emission of the electron is always followed by screening of the core hole [33–38]. Final state effects, which are mainly the result of screening of the core hole (called relaxation or rearrangement of charges) on binding energy after the photoemission event, must be included in the analysis and the inclusion decreases the initial state binding energies [34, 36–38]. It is therefore possible that order for the measured core level binding energies of cationic species in the XPS may not strictly follow $A^0 < A^{1+} < A^{2+} < A^{3+}$..... For instance, the order of the measured $2p_{3/2}$ core level binding energies for multiple cationic states of cobalt could increase as $Co^0 < Co^{3+} < Co^{2+}$, as a result of final state effects, particularly if we note that the Co XPS core level binding energies for CoO and Co_2O_3 might only differ within the margin of error so effectively that the binding energies for Co^{2+} is approximately the same as Co^{3+} [39]. Such a picture makes the possibility more likely that P_1 is assigned to the $+3$ cationic state and P_2 is the $+2$ cationic state or that P_1 is the $+2$ cationic state and P_2 is the $+3$ cationic state for one of the elements between A and B, but for the other element P_1 component corresponds to the $+3$ state while the P_2 component corresponds to the $+2$ state. As it is known that for an inverse spinel oxide of type AB_2O_4, the cations B^{3+} occupy tetrahedral sites and both cations A^{2+} and B^{3+} occupy octahedral sites, but practically speaking the tetrahedral and octahedral sites might contain multiple cationic states of both A and B elements. So, while in principle, all aforementioned assignments of the various cation component features might be possible, these different explanations cannot be reconciled. Importantly none of these explanations acknowledge that the surface or surface oxide might differ from the bulk and the resulting initial and final state effects might lead to different core level binding energies as a result of the surface being distinctly different from the bulk.

The surface of a solid material is chemically different from the bulk due to the lack of symmetry at the surface. The bonding environment of the atoms at the surface is different from the environment of the atoms in the bulk of the material, and such difference can cause shifts in core energy levels of the surface atoms compared to the bulk atoms [40]. Using the angle resolved x-ray photoelectron spectroscopy (ARXPS), Co and Fe $2p_{3/2}$ core levels of $CoFe_2O_4$ thin films have been shown to have surface weighted and bulk weighted components [41] in x-ray photoelectron spectra. Furthermore, the ratio between the components of the Co and Fe $2p_{3/2}$ core level spectra was found to depend on photoelectron emission angle (or photoemission angle) with respect to surface normal of the $CoFe_2O_4$ thin films, showing in a compelling fashion that there are surface weighted and bulk weighted components

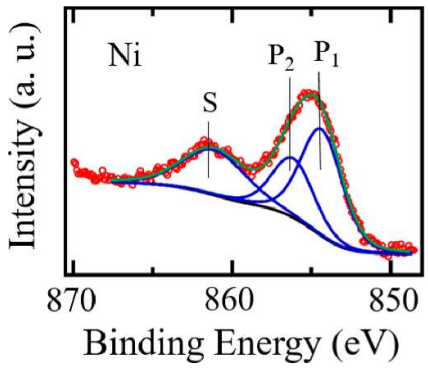

Figure 1. The XPS spectrum of the Ni $2p_{3/2}$ core level of a 10 nm thick $NiCo_2O_4$ (111) thin film. The raw spectrum (red circles) is fitted (green solid line) for three component peaks (blue solid lines): P_1, P_2, and S (satellite) peaks.

[41] in the x-ray photoelectron spectra of core levels. That study provided the evidence for the surface-to-bulk core level shifts in the binding energies of the Co and Fe $2p_{3/2}$ core levels in $CoFe_2O_4$ thin films. This surface-to-bulk core level shift does not, per se, exclude a surface oxide that differs from the bulk, so may include initial state effects, not just the expected surface enthalpy difference combined with final state effects [37, 40]. This prior study of $CoFe_2O_4$ thin films [41] does imply that the dependency of the ratio between surface weighted and bulk weighted components on the photoemission angle might be different for different spinel and inverse spinel oxide thin films. Furthermore, this prior work does not provide insight as to the role of the surface for a nanoparticle counterpart where the surface to volume ratio is significantly larger than for the spinel or inverse spinel oxide thin films.

2. Materials and methods

Epitaxial $NiFe_2O_4$ (111), $CoFe_2O_4$ (111), and $NiCo_2O_4$ (111) thin films, of 5 nm, 5 nm and 10 nm thicknesses respectively, were grown on Al_2O_3 (0001) substrates using pulsed laser deposition, as described elsewhere [4, 41]. For the inverse spinel oxides discussed here, there appears to be little variation in the XPS for the films of thicknesses of 5 nm or more [4, 41]. We have observed some deviations in the XPS, from the behavior seen with thicker films, in films of substantially less thickness than studied here ($\leqslant$2 nm) [4, 41] but the XPS on various thicknesses of samples is beyond the scope of this work and the much thinner films were not studied here. The $Ni_xCo_{1-x}Fe_2O_4$ (x = 0, 0.2, 0.5, 0.8, 1) nanoparticles were synthesized using a microwave assisted process. Nickel nitrate ($Ni(NO_3)_2.6H_2O$), cobalt nitrate ($Co(NO_3)_2.6H_2O$), and iron acetate ($Fe(CO_2CH_3)_2$) from Sigma Aldrich were used as the precursor materials for the synthesis of the nanoparticles. Stoichiometric ratios of precursor materials were dissolved in 40 ml of ethylene glycol followed by continuous stirring and heating at 65 °C for 3 h to create a homogenous solution. Next, the resulting homogeneous solution was kept in the CEM microwave reactor and irradiated for 30 min at 180° C with 100 mW power. Distilled water was then added to the solution and kept overnight for precipitation. The precipitates were washed with distilled water and separated by centrifugation. The precipitates were then dried in an oven at 200° C. The dried precipitates were crushed into fine powder and calcined at 600 °C for 5 h in a tube furnace. To analyze the particle size of nanoparticles scanning electron microscopy (SEM) was done on Helios NanoLab Dual Beam 660. First, 0.2 mg of nanoparticles were dispersed in 15 ml ethanol and sonicated for 10 min. Then a small amount of the dispersion was drop-cast on carbon tape using a dropper. The films of nanoparticles on carbon tape were analyzed on SEM. It was found that the cobalt ferrite nanoparticles follow a normal distribution of particle size i.e. particle diameter with mean diameter of 73 nm as shown in figure 2. But the nickel ferrite nanoparticles followed a bimodal distribution of particle diameter with mean of 21 nm and 69 nm (see figure S1 of the supplementary information). These particle sizes are in much the same range as prior studies (20–70 nm) of cobalt nickel ferrite nanoparticles [42]. The $Ni_xCo_{1-x}Fe_2O_4$ (x = 0, 0.2, 0.5, 0.8, 1) nanoparticles crystallite sizes, determined from x-ray diffraction (see the supplementary materials figure S2), were 14.4 nm, 11.9 nm, 11.7 nm, 9.0 nm and 12.4 nm for x = 0, 0.2, 0.5, 0.8, 1 respectively. The crystallite size calculated from x-ray diffraction data are smaller than the particle size determined from the SEM, but as we know the crystallite size depends upon the coherently diffracted domain size which may often be smaller than the particle size.

The magnetic hysteresis loops were measured for the $CoFe_2O_4$ and $NiCo_2O_4$ nanoparticles in a super conducting quantum interference device (SQUID) magnetometer (MPMS XL SQUID magnetometer from Quantum Design), as a function of temperature, while the entire range of $Ni_xCo_{1-x}Fe_2O_4$ (x = 0, 0.2, 0.5, 0.8, 1) nanoparticles were also characterized by vibrating sample magnetometry (VSM). VSM magnetometry data for the five samples ($CoFe_2O_4$, $NiFe_2O_4$, $Ni_{0.2}Co_{0.8}Fe_2O_4$, $Ni_{0.5}Co_{0.5}Fe_2O_4$, $Ni0_{0.8}Co_{0.2}Fe_2O_4$) were collected using a Quantum Design VersaLab 3 Tesla cryogen-free VSM at 300 K. In the ferrimagnetic systems at zero magnetic field, spin moments with larger and smaller magnitudes are oppositely aligned. When the magnetic field is applied, changing from zero field, the rotation of the oppositely aligned spin moments results in a characteristic feature for a ferrimagnet at higher magnetic fields, much higher than the apparent coercive magnetic field. These effects that broaden the magnetic hysteresis to higher fields was observed in the hysteresis measurements of the nanoparticles, and the feature is much noticeable especially in the hysteresis of $CoFe_2O_4$ nanoparticles (see figure S3 in the supplementary information). For both $CoFe_2O_4$ and $NiCo_2O_4$ nanoparticles, the moments in general saturated at lower field and saturation magnetization was larger at lower temperatures. The measured remanent magnetization of the $Ni_xCo_{1-x}Fe_2O_4$ (x = 0, 0.2, 0.5, 0.8, 1) nanoparticles decreases with increasing nickel concentrations, as was seen in prior cobalt nickel ferrite nanoparticles studies [42].

The x-ray photooemission spectra for the $CoFe_2O_4$ thin films and $CoFe_2O_4$ nanoparticles were acquired using a SPECS x-ray Mg Kα anode (hv = 1253.6 eV) source

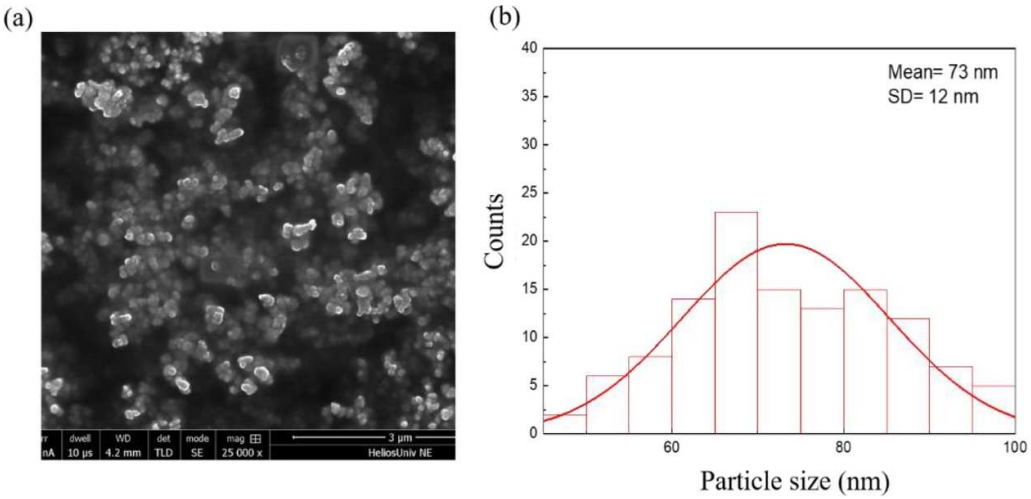

Figure 2. (a) The scanning electron microscopy (SEM) images of $CoFe_2O_4$ nanoparticles. (b) The distribution of the $CoFe_2O_4$ nanoparticles sizes, for the nanoparticles studied here.

and VG100AX hemispherical analyzer using a pass energy of 50 eV. For the $NiFe_2O_4$ and $NiCo_2O_4$ thin films and $Ni_xCo_{1-x}Fe_2O_4$ nanoparticles, the XPS measurements were carried out using a SPECS x-ray Al Kα anode (hv = 1486.6 eV) source and PHOIBOS 150 energy analyzer with 13 eV pass energy. At room temperature, ARXPS measurements on thin films were carried out at six different photoemission angles with respect to the surface normal (0°). The XPS hemispherical analyzer has an acceptance angle of ±10°. At each photoemission angle, the binding energies of the various XPS core level components are referenced to the adventitious C 1s position to eliminate variations in binding energies due to photovoltaic surface charging. The uncertainty in binding energy measurement in this work is ±0.1 eV. The limited electron mean free path ensures that by changing the photoelectron emission angle, the ARXPS can be used to distinguish components in the XPS spectra that have greater surface weight, i.e. larger photoemission angles with respect to the surface normal of the sample result in core level photoelectron spectra with greater surface weights (see figure S4 of the supplementary information) [43].

3. Results and discussions

3.1. XPS of selected Ni and Co spinel ferrites: thin films versus nanoparticles

Figure 3 shows the ARXPS of a $NiFe_2O_4$ (111) thin film. The Ni $2p_{3/2}$ core level spectra were fitted for three components: P_1 at 854.7 eV, P_2 at 856.5 eV, and S (satellite) at 861.6 eV. The main core level peak of the Ni $2p_{3/2}$, at normal photoemission, was observed to be at a binding energy of 855.2 eV which is in excellent agreement with the value reported elsewhere [39]. The Fe $2p_{3/2}$ core level spectra are fitted for two components: P_1 at 710.5 eV and P_2 at 712.3 eV. The main Fe $2p_{3/2}$ core level spectral feature, at normal emission, was observed to be at 711.5 eV, which is found to be higher than the value found elsewhere [44]. For the component fits to the ARXPS spectra, the widths of all the component peaks and peak positions of the components P_1 and P_2 are fixed at all angles so that any changes in the spectral features, as photoemission angle changes, could be ascribed to surface weighted or bulk weighted feature. As the photoemission angle increases, we observed that intensity of P_1 component relative to P_2 of both Ni and Fe core levels increases, showing that P_1 (P_2) is a surface (bulk) weighted component of the core levels. The binding energy shift between components P_1 and P_2, which is 1.8 eV, is therefore an effective surface-to-bulk core level shift. Figure 4 shows that the P_1/P_2 intensity ratios for both Ni and Fe core levels increase, as photoemission angle increases, and become maximum at the largest take-off angle, with respect to the surface normal, measured here (50°). The XPS characterization at larger (smaller) photoemission angles in this work gives the more surface (bulk) weighted character (see figure S4 of the supplementary information). The consequence of the effective surface-to-bulk core level shifts observed for the $NiFe_2O_4$ thin film is that the main peaks of the XPS spectra of both Ni and Fe core levels at 50°, when compared with the main XPS spectral peaks at 0°, are shifted toward the side of surface weighted component, which in this case is lower binding energy side (see figure S5 of the supplementary information).

ARXPS is most meaningful where the change in the photoelectron emission angle is representative of a change of the electron mean free path component along the surface normal. For the systems like nanoparticles, the ARXPS technique is physically less meaningful because of inhomogeneities between different particles and more random multiple surface directions of different particles. A comparative study between thin films and their nanoparticle counterparts is best done by comparing XPS spectra with the emission angle along the surface normal as this contains both surface and more bulk components, and for the nanoparticles, might be considered more of an average of the chemical or electronic properties representative of nanoparticles.

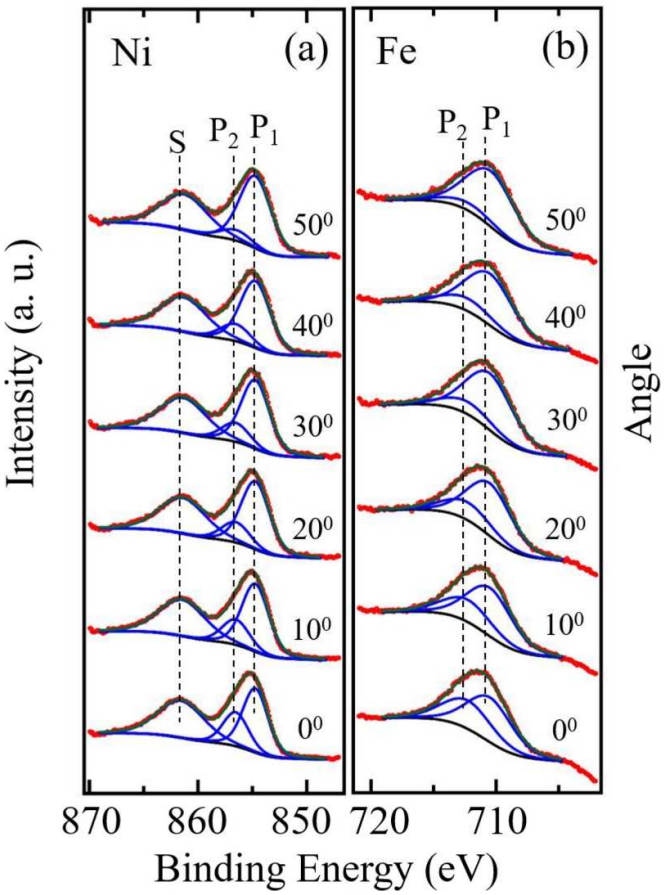

Figure 3. The ARXPS of a $NiFe_2O_4$ (111) thin film. Shown are the XPS spectra of (a) Ni $2p_{3/2}$ and (b) Fe $2p_{3/2}$ core levels at six different photoemission angles with respect to the surface normal of the sample. Red circles, green solid lines, and blue solid lines represent raw spectra, fit of the data, and components of the spectra respectively. Spectra at higher angles are normalized to the normal emission (0°) photoelectron spectra.

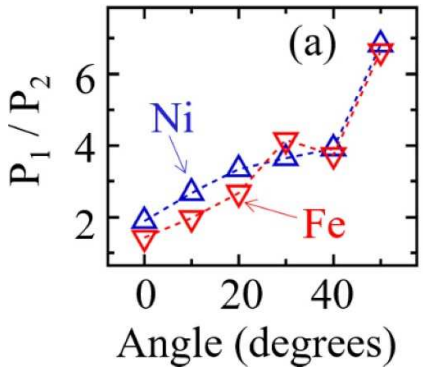

Figure 4. The dependency of the ratio between P_1 and P_2 components of the Ni $2p_{3/2}$ core level (blue upright triangles) and the Fe $2p_{3/2}$ core level (red inverted triangles) spectra on photoemission angle supporting a surface-to-bulk core level shifts in $NiFe_2O_4$ (111) thin films.

Figure 5 shows the comparison of normal emission XPS (photoemission angle is 0°) core level spectra of some ferrite nanoparticles of type $Ni_xCo_{1-x}Fe_2O_4$ ($x = 0.2, 0.5, 0.8, 1$) with that of $NiFe_2O_4$ (111) thin film. This comparison shows

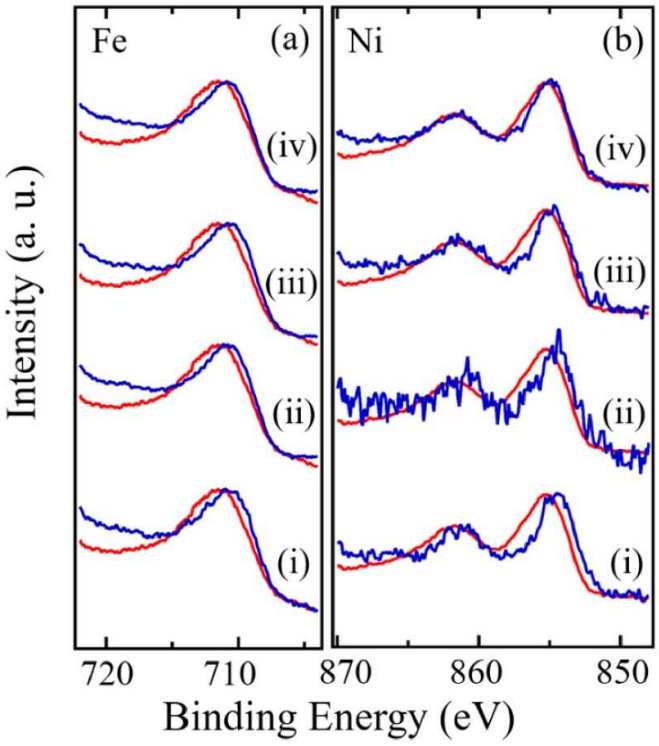

Figure 5. A comparison of normal emission XPS spectra of the (a) Fe and (b) Ni $2p_{3/2}$ core levels in some spinel oxide nanoparticles with that observed for the $NiFe_2O_4$ (111) thin film. The blue spectra are the XPS core level spectra for (i) $NiFe_2O_4$, (ii) $Ni_{0.2}Co_{0.8}Fe_2O_4$, (iii) $Ni_{0.5}Co_{0.5}Fe_2O_4$, and (iv) $Ni_{0.8}Co_{0.2}Fe_2O_4$ nanoparticles, and red spectra are the normal emission XPS core level spectra for a $NiFe_2O_4$ thin film.

that main $2p_{3/2}$ core level peaks for both Fe and Ni of all nanoparticles are shifted to lower binding energies compared to the corresponding peaks of $NiFe_2O_4$ (111) thin film. These core level shifts suggests that the nanoparticles, on average, chemically and electronically behave similar to the atoms at the surface of $NiFe_2O_4$ thin film, i.e. dominated by the more surface transition metal $2p_{3/2}$ XPS P_1 components, so the nanoparticle on average should, electronically, be dominated by the surface and thus more resemble the surface of their thin film counterparts. In another words, the $Ni_xCo_{1-x}Fe_2O_4$ ($x = 0.2, 0.5, 0.8, 1$) type nanoparticles are chemically or electronically different from the bulk of $NiFe_2O_4$ thin films. In the comparison between the thin films and nanoparticles, as shown in figure 5, the P_1 components (see figure 3) of the $2p_{3/2}$ core level spectra, for the nanoparticles, exhibit a much larger intensity than the intensity of P_2 component of the Fe and Ni $p_{3/2}$ core level spectra. This relative enhancement of the P_1 components, of the nanoparticle $2p_{3/2}$ core level spectra, is evident in the fitting of the XPS core level spectra components for the $NiFe_2O_4$ thin films and nanoparticle specimens (see figure S6 of the supplementary information).

Similar ARXPS measurements were carried out on $CoFe_2O_4$ (111) thin films. Figure 6 shows some representative ARXPS Co and Fe $2p_{3/2}$ core level spectra from a $CoFe_2O_4$ (111) thin film. The Co $2p_{3/2}$ core level spectra contain three component peaks: P_1 at 779.4 eV, P_2 at 781.4 eV and S

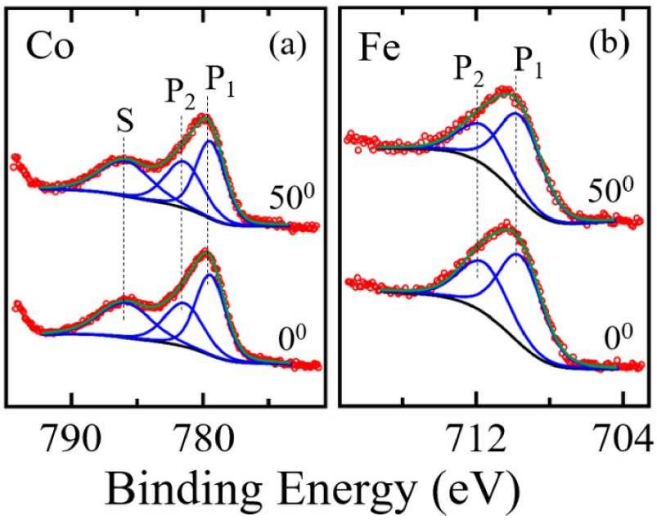

Figure 6. Some representative XPS core level spectra of the (a) Co $2p_{3/2}$ and (b) Fe $2p_{3/2}$ of a $CoFe_2O_4$ (111) thin film for photoemission angles of 0° and 50° with respect to the surface normal are shown. In the figure, red circles, green solid lines, blue solid lines, and black solid lines are raw data, fitted lines, component peaks, and background levels respectively.

(satellite) at 785.9 eV binding energies. At normal emission (0°), the main peak position of the Co $2p_{3/2}$ core level was found to be at a binding energy of 779.7 eV which is in excellent agreement with the 779.9 ± 0.2 eV reported elsewhere [39]. The Fe $2p_{3/2}$ core level spectra contains two component peaks: P_1 at binding energies of 709.6 eV and P_2 at 711.6 eV. The main peak position of Fe $2p_{3/2}$ core level at normal emission was found to be at a binding energy of 710.3 eV which is in good agreement with the binding energy value of 710.6 ± 0.2 eV, as reported elsewhere [43]. As the photoelectron emission angle increases with respect to the normal, the ratios of the XPS core level component peaks change: the P_1/P_2 intensity ratio values for the Co (Fe) $2p_{3/2}$ core level decreased (increased) when the photoemission angle was increased, as shown in figures 7 (a) and (b), indicating that P_1 (P_2) of Co (Fe) core level is a bulk weighted component, and P_2 (P_1) of Co (Fe) core level is a surface weighted component. In simple terms, the surface must again be somewhat distinct from the bulk in $CoFe_2O_4$ (111) thin films.

Although an intensity ratio (P_1/P_2) dependency was observed for the P_1 and P_2 components of the Co and Fe $2p_{3/2}$ core level spectra of $CoFe_2O_4$ (111) thin films, as a function of photoemission angle as illustrated in figures 7(a) and (b), the intensity ratio changes from normal emission to a large take-off angle, 0° to 50°, were not as large as compared to the ratio change observed for $NiFe_2O_4$ thin films. The change in the P_1/P_2 component ratio for $CoFe_2O_4$ (111) is not large enough to appreciably show shifts of the spectra taken at 50° relative to the spectra taken at 0°, as is evident in figures 7(c) and (d). Unlike the ARXPS of the $NiFe_2O_4$ (111) thin film, no noticeable shifts of the core level spectra taken at 50° towards the surface component side of the spectra taken at 0° was observed. When the $2p_{3/2}$ core level XPS spectra of the $CoFe_2O_4$ (111) thin film are compared to those of $CoFe_2O_4$ nanoparticles, as shown in figures 7(e) and (f), the $CoFe_2O_4$ thin film and nanoparticles imply that the nanoparticles have XPS signatures more like the bulk of $CoFe_2O_4$ thin film because the nanoparticle spectra are apparently shifted to now the P_1 bulk component of the Co $2p_{3/2}$ spectra. These signatures are, however, not overly compelling.

Table 1 lists the estimated core level binding energies and the stoichiometry of all oxide thin films and nanoparticles studied here. From the apparent stoichiometry, estimated from the core level intensities after corrections for cross section and the transmission of the electronic energy analyzer, several general features are observed: the surface is Ni rich compared to Co in the $Ni_xCo_{1-x}Fe_2O_4$ type ferrite nanoparticles, and the surface concentration ratio of Fe to the other cationic species together in the system is higher in ferrite nanoparticles than in thin films. Roughly, the estimated stoichiometry, from table 1, suggests that the ferrite nanoparticles have the concentration ratio of Fe to all other cationic species closer to the expected ratio of 2:1 as compared to the thin film ferrites. Ideally, ratio of concentration of Fe relative to other cationic species should be 2:1 in these ferrites, but the ratio is much less than one in the stoichiometry for thin film ferrites, as estimated from the experimental intensities obtained from XPS.

In order to provide a comparison between ferrite thin films and another spinel oxide thin film of similar structure, we present the study of ARXPS on $NiCo_2O_4$ thin film in the following section.

3.2. ARXPS of the $NiCo_2O_4$ thin film

For the purpose of comparison, a closer examination was given to the $NiCo_2O_4$ crystalline thin films. Like the ferrites under the study, $NiCo_2O_4$ also exists in the inverse spinel structure. Figure 8 shows the $2p_{3/2}$ core level XPS spectra of Ni and Co for $NiCo_2O_4$ (111). The Ni $2p_{3/2}$ core level spectra contain three component peaks: P_1 at 854.4 eV, P_2 at 856.2 eV and the satellite feature S at 861.1 eV. At normal emission (0°), the main peak position of the Ni $2p_{3/2}$ core level is found to be at a binding energy of 855.0 eV. The Co $2p_{3/2}$ level contains three components too: P_1 at 779.7 eV, P_2 at 781.5 eV, and S (satellite) at 785.5 eV. The main peak position of the Co $2p_{3/2}$ core level at normal emission is found to be at a binding energy of 780.1 eV. The main peak positions of both Ni and Co $2p_{3/2}$ core levels are comparable but somewhat larger than the values of core level binding energies reported elsewhere [45].

An effective surface-to-bulk core level shifts was observed for the $NiCo_2O_4$ thin films. This is evident as there are higher values for the component ratios P_1/P_2 of both Ni and Co $2p_{3/2}$ core levels at higher photoemission angles, on average, as shown in figure 9(a) and (b). The component P_1 (P_2) is a surface (bulk) component of the core levels and the surface-to-bulk core level shifts was observed to be 1.8 eV, which is similar to the shifts observed for the $NiFe_2O_4$ thin films discussed above. The $NiCo_2O_4$ thin film surface was found to be Ni rich, as indicated by the estimated surface

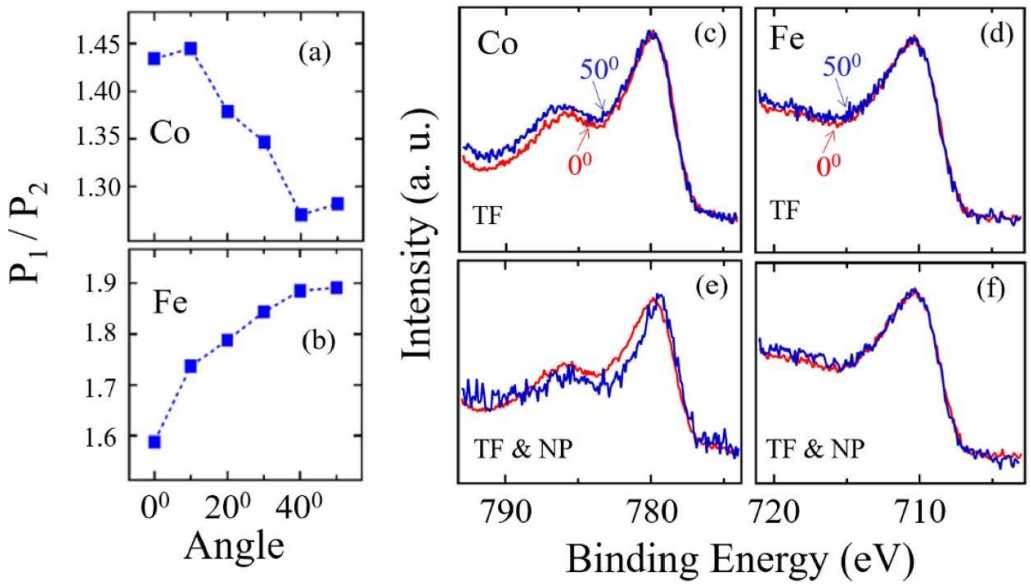

Figure 7. The P_1/P_2 component intensity ratios for the (a) Co and (b) Fe $2p_{3/2}$ core level as a function of photoemission angle. The comparison of the (c) Co and (d) Fe $2p_{3/2}$ core level spectra of a $CoFe_2O_4$ (111) thin film (TF) between small and large, 0° and 50°, photoemission angles. The comparison of (c) Co and (d) Fe $2p_{3/2}$ core level spectra between a $CoFe_2O_4$ (111) thin film and the corresponding nanoparticles (NP). In (e) and (f) red and blue spectra are for $CoFe_2O_4$ thin film and nanoparticles respectively.

Table 1. The estimated surface stoichiometry and core level binding energies of the thin film (TF) and nanoparticles (NP) samples under the study.

Sample stoichiometry		Measured core level binding energy (eV) of			
Expected	Estimated for surface (using XPS)	Ni $2p_{3/2}$	Co $2p_{3/2}$	Fe $2p_{3/2}$	Component of lattice site oxygen (O^{2-}) in O 1s
$Ni_{0.2}Co_{0.8}Fe_2O_4$ (NP)	$Ni_{0.20}Co_{0.50}Fe_{1.89}O_{4.51}$	854.6	780.1	710.8	529.3
$Ni_{0.5}Co_{0.5}Fe_2O_4$ (NP)	$Ni_{0.63}Co_{0.29}Fe_{1.66}O_{4.32}$	854.8	780.4	710.7	529.1
$Ni_{0.8}Co_{0.2}Fe_2O_4$ (NP)	$Ni_{1.03}Co_{0.15}Fe_{1.62}O_{4.19}$	854.9	780.3	710.8	529.3
$NiFe_2O_4$ (NP)	$Ni_{0.70}Fe_{1.44}O_{4.85}$	854.5		710.7	529.3
$CoFe_2O_4$ (NP)	$Co_{1.24}Fe_{1.79}O_{3.96}$		779.4	710.3	529.4
$NiFe_2O_4$ (TF)	$Ni_{2.50}Fe_{0.87}O_{3.64}$	855.2		711.5	529.5
$CoFe_2O_4$ (TF)	$Co_{2.09}Fe_{1.01}O_{3.89}$		779.8	710.3	529.3
$NiCo_2O_4$ (TF)	$Ni_{1.3}Co_{1.8}O_{3.8}$	855.0	779.7		529.7

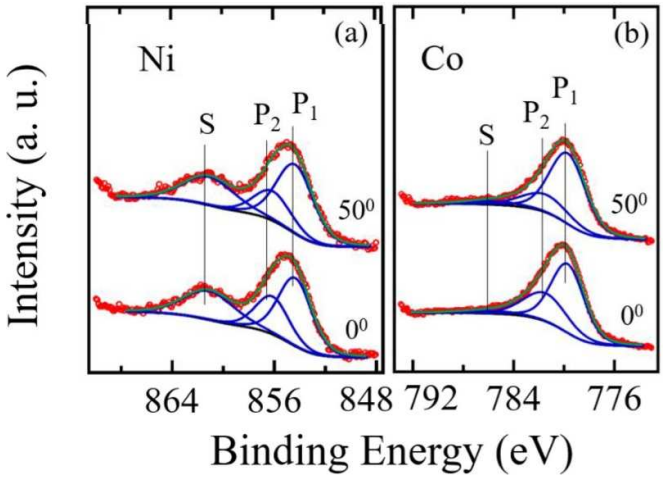

Figure 8. The angle resolved x-ray photoelectron spectroscopy of a 10 nm thick $NiCo_2O_4$ (111) thin film. (a) The Ni $2p_{3/2}$ and (b) Co $2p_{3/2}$ XPS core level spectra taken at photoemission angles of 0° and 50° with respect to the surface normal of the sample.

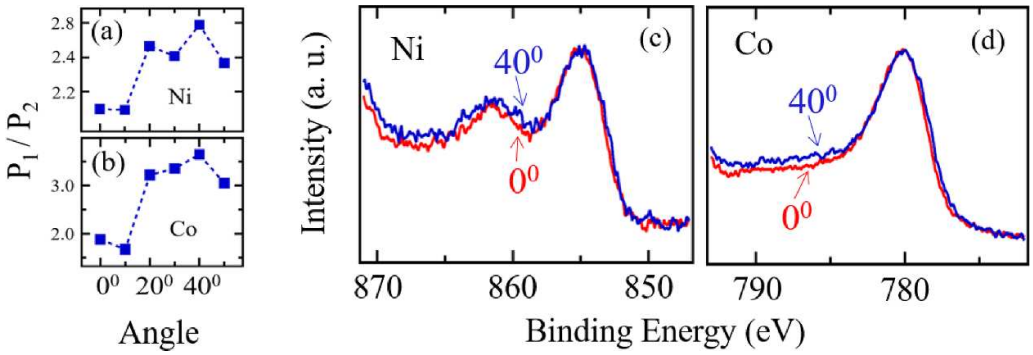

Figure 9. A summary of the effective surface-to-bulk core level shifts in $NiCo_2O_4$ (111) thin film. (a) Dependency of the ratio between P_1 and P_2 of the (a) Ni and (b) Co $2p_{3/2}$ core levels on photoemission angle. (c) Ni and (c) Co $2p_{3/2}$ XPS spectra at 40° photoemission angle, compared to the corresponding XPS spectra taken at 0° photoemission angle.

stoichiometry of $Ni_{1.3}Co_{1.8}O_{3.8}$. $NiCo_2O_4$ thin film, similar to the ferrite thin films reported here, is observed to have surface-to-bulk core level shifts and, on comparing $NiCo_2O_4$ to AB_2O_4, the 'A' type cation is observed to be rich at surface, which is again observed for ferrite thin films under study here.

Although clear dependencies of the component intensity ratios (P_1/P_2), for each cation of three inverse spinel oxide thin films, were observed on the photoemission angle, indicating surface-to-bulk core level shifts, the degree of the dependency was not the same for each of the thin films. In order to better understand the nature of the thin film surfaces, adventitious carbon (AdC) 1s and oxygen core level O 1s were analyzed for all three thin films. The analyses showed that $NiFe_2O_4$ thin film surface had lower number of adsorbed contamination species compared to the $CoFe_2O_4$ and $NiCo_2O_4$ thin film surfaces (see figures S7–S9 of the supplementary information). It is possible that relatively lower degree of dependencies of the component intensity ratios (P_1/P_2) on photoemission angle for $CoFe_2O_4$ and $NiCo_2O_4$ thin films could be due to larger number of contamination species at the surfaces.

In the XPS spectra of all the inverse spinel oxides studied here, the satellite feature intensity for the core level spectra of nominally second transition metal cation B^{3+} is significantly suppressed. For instance, the core level spectra of Fe in ferrites and Co in $NiCo_2O_4$ do not have an appreciable satellite intensity, although some non-zero intensity for the Co satellite component was inferred from the data for the $NiCo_2O_4$ thin film. Satellite features are ascribed to the presence of two-hole final state [36], one of the multiple final states of the system in photoemission, which effectively increases nuclear charge and decreases the kinetic energy of the photoelectron, thereby leading to the increased binding energy component for the satellite feature [36]. Suppression of the satellite intensity indicates that the two-hole final state is suppressed for +3 cationic species. The XPS spectra show suppressed satellite intensities for the Fe $2p_{3/2}$ core levels of $NiFe_2O_4$ and $CoFe_2O_4$ where the Fe cation is nominally 3+ ($3d^5$) and for the Co $2p_{3/2}$ core levels of $NiCo_2O_4$ where the Co cation is nominally 3+ ($3d^6$) [3]. We found especially for Co in $NiCo_2O_4$ that annealing the system at certain higher temperature could enhance the intensity for satellite components (see figure S10 of the supplementary information), suggesting that two-hole final state could be activated by annealing.

4. Conclusions

We observed, using ARXPS, that a surface and a bulk weighted components can be distinguished in the $2p_{3/2}$ core level spectra of the various cations in some inverse spinel oxide thin films. That some $2p_{3/2}$ core level spectral components are more surface or bulk weighted lead to what may be considered as an effective surface-to-bulk core level shifts in the transition metal $2p_{3/2}$ core level spectra from these inverse spinel oxide thin films. In the ARXPS of $NiFe_2O_4$ thin film, an appreciable dependence of the core level surface and bulk weighted component ratios, on the photoemission angle, indicates that the surface of $NiFe_2O_4$ thin film is chemically different from the bulk. The nanoparticles of type $Ni_xCo_{1-x}Fe_2O_4$ ($x = 0.2, 0.5, 0.8, 1$) may also chemically be similar to oxides seen at the surface of $NiFe_2O_4$ thin films. From ARXPS, the dependencies of the $2p_{3/2}$ core level component ratios on photoemission angle for $CoFe_2O_4$ and $NiCo_2O_4$ thin films were not observed to be as appreciable as was observed for $NiFe_2O_4$ thin film, possibly due to higher contaminant species present at the surface of $CoFe_2O_4$ and $NiCo_2O_4$ thin films. In addition, the surfaces could be richer in A-type atoms in the inverse spinel oxide thin films of type AB_2O_4, and proportion between the cationic species in the thin film systems could be farther from the ideal proportion, compared to the inverse spinel oxide nanoparticle systems. The deviations from the expected composition, as seen in XPS, are because the surface composition differs from the bulk, as is so often the case with oxides [46–48]. This is consistent with the fact that some of the various transition metal $2p_{3/2}$ core level components have surface weight. The overall stoichiometry of the inverse spinel oxide films is as expected, as is the structure of the bulk of the film. There can be now no guarantee that the surface oxidation state is the same as the bulk.

Data availability statements

All data that support the findings of this study are included within the article (and any supplementary files).

Acknowledgments

This work was supported by the National Science Foundation (NSF) through the EPSCoR RII Track-1: Emergent Quantum Materials and Technologies (EQUATE), Award Number OIA-2044049 and NSF-PREM Award Number 1827690.

CRediT authorship contribution statement

Sample Preparation: D Y, X X, S S, P Y, and V R; Data Acquisition: A S, D Y, W K C, R M, B T, S S, R Y L and P Y; Data Analysis: A S, and R M; Data Curation: A S and P A D; Manuscript Preparation: A S; Final Manuscript Preparation: A S and P A D; Project Supervision: X X, V R, R Y L, J S, and P A D; Funding: X X, V R, R Y L, J S, and P A D.

Conflict of interest

The authors declare that they have no known competing financial and personal relationships with other people or organizations that could inappropriately influence (bias) their work.

ORCID iDs

Arjun Subedi https://orcid.org/0000-0002-7581-8144
Wai Kiat Chin https://orcid.org/0000-0002-1840-0825
Rebecca Y Lai https://orcid.org/0000-0002-1732-9481
Xiaoshan Xu https://orcid.org/0000-0002-4363-392X
Peter A Dowben https://orcid.org/0000-0002-2198-4710
Vijaya Rangari https://orcid.org/0000-0002-3962-1686

References

[1] Jauhar S, Kaur J, Goyal A and Singhal S 2016 Tuning the properties of cobalt ferrite: a road towards diverse applications *RSC Adv.* **6** 97694–719
[2] Narang S B and Pubby K 2021 Nickel spinel ferrites: a review *J. Magn. Magn. Mater.* **519** 167163
[3] Xu X, Mellinger C, Cheng Z G, Chen X and Hong X 2022 Epitaxial $NiCo_2O_4$ film as an emergent spintronic material: magnetism and transport properties *J. Appl. Phys.* **132** 020901
[4] Yang D, Yun Y, Subedi A, Rogers N E, Cornelison D M, Dowben P A and Xu X 2021 Colossal intrinsic exchange bias from interfacial reconstruction in epitaxial $CoFe_2O_4/Al_2O_3$ thin films *Phys. Rev.* B **103** 224405
[5] Mellinger C, Wang X, Subedi A, Clark A T, Komesu T, Rosenberg R, Dowben P A, Cheng X and Xu X 2023 Interfacial and surface magnetism in epitaxial $NiCo_2O_4(001)/MgAl_2O_4$ films *J. Appl. Phys.* **133** 195301
[6] Solís C, Toldra-Reig F, Balaguer M, Somacescu S, Garcia-Fayos J, Palafox E and Serra J M 2018 Mixed ionic–electronic conduction in $NiFe_2O_4$–$Ce_{0.8}Gd_{0.2}O_{2-\Delta}$ nanocomposite thin films for oxygen separation *ChemSusChem* **11** 2818–27
[7] Wang W, Du Q, Wang B, Li Y, Hu Z, Wang Y, Wang Z and Liu M 2022 Manipulated magnetic coercivity and spin reorientation transition in $NiCo_2O_4$ films *J. Appl. Phys.* **132** 073901
[8] Gao M, Le K, Du W, Wang Z, Wang F, Liu W and Liu J 2019 Enhanced supercapacitive performance of the $CoFe_2O_4/CoFe_2S_4$ composite nanoflake array induced by surface sulfidation *New J. Chem.* **43** 13491–8
[9] Lee J H, Noh Y W, Jin I S, Park S H and Jung J W 2019 Efficient perovskite solar cells with negligible hysteresis achieved by sol-gel-driven spinel nickel cobalt oxide thin films as the hole transport layer *J. Mater. Chem.* C **7** 7288–98
[10] Wang S, Wang L, Liu C, Shan Y, Li F and Sun L 2022 $NiCo_2O_4$ thin film prepared by electrochemical deposition as a hole-transport layer for efficient inverted perovskite solar cells *RSC Adv.* **12** 12544–51
[11] Li L, Ma Z, Liu L, Wang X, Wang J, Cao L Y, Liu S and Zhang W 2022 $NiCo_2O_4$/carbon nanofibers composite as an efficient counter electrode for dye-sensitized solar cells *Mater. Res. Bull.* **145** 111528
[12] Ouyang D, Xiao J, Ye F, Huang Z, Zhang H, Zhu L, Cheng J and Choy W C H 2018 Strategic synthesis of ultrasmall $NiCo_2O_4$ NPs as hole transport layer for highly efficient perovskite solar cells *Adv. Energy Mater.* **8** 1702722
[13] Liu J, Meng R, Li J, Jian P, Wang L and Jian R 2019 Achieving high-performance for catalytic epoxidation of styrene with uniform magnetically separable $CoFe_2O_4$ nanoparticles *Appl. Catal.* B **254** 214–22
[14] Liu Y, Chi X, Han Q, Du Y, Yang J and Liu Y 2019 Vertically self-standing C@$NiCo_2O_4$ nanoneedle arrays as effective binder-free cathodes for rechargeable Na−O_2 batteries *J. Alloys Compd.* **772** 693–702
[15] Zhang R, Liu M, Liu W and Wang H 2017 Highly conductive n-type $NiCo_2O_{4-\delta}$ epitaxial thin films grown by RF sputtering *Mater. Lett.* **199** 164–7
[16] Kang P, Zhou G, Ji H, Li Z, Li Z and Xu X 2022 Emergence of room-temperature perpendicular magnetic anisotropy in metallic $NiCo_2O_4$ thin film *J. Magn. Magn. Mater.* **553** 169293
[17] Bacelis-Martínez R D, Oskam G, Rodriguez Gattorno G and Ruiz-Gómez M A 2017 Inkjet printing as high-throughput technique for the fabrication of $NiCo_2O_4$ Films *Adv. Mater. Sci. Eng.* **2017** 1–9
[18] Liu Z, Zhen C, Xu D, Wu X, Wang H, Ma L, Zhao D, Tian Z and Hou D 2020 Significantly enhanced photocurrent density in $NiCo_2O_4$/a-C/Si photoanode for water splitting *Appl. Surf. Sci.* **529** 147155
[19] Marco J F, Gancedo J R, Gracia M, Gautier J L, Ríos E I, Palmer H M, Greaves C and Berry F J 2001 Cation distribution and magnetic structure of the ferrimagnetic spinel $NiCo_2O_4$ *J. Mater. Chem.* **11** 3087–93
[20] Gao L, Han E, He Y, Du C, Liu J and Yang X 2020 Effect of different templating agents on cobalt ferrite ($CoFe_2O_4$) nanomaterials for high-performance supercapacitor *Ionics* **26** 3643–54
[21] Aghavnian T, Moussy J B, Stanescu D, Belkhou R, Jedrecy N, Magnan H, Ohresser P, Arrio M A, Sainctavit P and Barbier A 2015 Determination of the cation site distribution of the spinel in multiferroic $CoFe_2O_4/BaTiO_3$ layers by x-ray photoelectron spectroscopy *J. Electron. Spectrosc. Relat. Phenom.* **202** 16–21
[22] Yao H, Ning X, Zhao H, Hao A and Ismail M 2021 Effect of Gd-doping on structural, optical, and magnetic properties of $NiFe_2O_4$ As-prepared thin films via facile Sol-Gel approach *ACS Omega* **6** 6305–11
[23] Yadav R S, Kuřitka I, Vilcakova J, Havlica J, Masilko J, Kalina L, Tkacz J, Enev V and Hajdúchová M 2017

Structural, magnetic, dielectric, and electrical properties of $NiFe_2O_4$ spinel ferrite nanoparticles prepared by honey-mediated sol-gel combustion *J. Phys. Chem. Solids* **107** 150–61

[24] Hao A, Ismail M, He S, Qin N, Chen R, Rana A M and Bao D 2018 Enhanced resistive switching and magnetic properties of Gd-doped $NiFe_2O_4$ thin films prepared by chemical solution deposition method *Mater. Sci. Eng.* **229** 86–95

[25] Kumar Y, Sharma A and Shirage P M 2019 Impact of different morphologies of $CoFe_2O_4$ nanoparticles for tuning of structural, optical and magnetic properties *J. Alloys Compd.* **778** 398–409

[26] Wang W P, Yang H, Xian T and Jiang J L 2012 XPS and magnetic properties of $CoFe_2O_4$ nanoparticles synthesized by a polyacrylamide gel route *Mater. Trans.* **53** 1586–9

[27] Lee G, Jeong M, Kim H R, Kwon M, Baek S, Oh S, Lee M, Lee D and Joo J H 2022 Controlled electrophoretic deposition strategy of binder-free $CoFe_2O_4$ nanoparticles as an enhanced electrocatalyst for the oxygen evolution reaction *ACS Appl. Mater. Interfaces* **14** 48598–608

[28] Zhou Z, Zhang Y, Wang Z, Wei W, Tang W, Shi J and Xiong R 2008 Electronic structure studies of the spinel $CoFe_2O_4$ by x-ray photoelectron spectroscopy *Appl. Surf. Sci.* **254** 6972–5

[29] Prieto P, Marco J F, Prieto J E, Ruiz-Gomez S, Perez L, Del Real R P, Vázquez M and de la Figuera J 2018 Epitaxial integration of $CoFe_2O_4$ thin films on Si (001) surfaces using TiN buffer layers *Appl. Surf. Sci.* **436** 1067–74

[30] Liu N, Du P, Zhou P, Tanguturi R G, Qi Y, Zhang T and Zhuang C 2020 Annealing temperature effects on the cation distribution in $CoFe_2O_4$ nanofibers *Appl. Surf. Sci.* **532** 147440

[31] Panwar K, Tiwari S, Bapna K, Heda N L, Choudhary R J, Phase D M and Ahuja B L 2017 The effect of Cr substitution on the structural, electronic and magnetic properties of pulsed laser deposited $NiFe_2O_4$ thin films *J. Magn. Magn. Mater.* **421** 25–30

[32] Jaffari G H, Rumaiz A K, Woicik J C and Shah S I 2012 Influence of oxygen vacancies on the electronic structure and magnetic properties of $NiFe_2O_4$ thin films *J. Appl. Phys.* **111** 093906

[33] Bagus P S, Illas F, Pacchioni G and Parmigiani F 1999 Mechanisms responsible for chemical shifts of core-level binding energies and their relationship to chemical bonding *J. Electron. Spectrosc. Relat. Phenom.* **100** 215–36

[34] Bagus P S, Ilton E S and Nelin C J 2013 The interpretation of XPS spectra: insights into materials properties *Surf. Sci. Rep.* **68** 273–304

[35] Bagus P S, Ilton E and Nelin C J 2018 Extracting chemical information from XPS spectra: a perspective *Catal. Lett.* **148** 1785–802

[36] Hufner S 2003 *Photoelectron Spectroscopy Principles and Applications* 3rd edn (Springer)

[37] Dowben P A 2000 The metallicity of thin films and overlayers *Surf. Sci. Rep.* **40** 151–247

[38] Egelhoff Jr W F 1987 Core-level binding-energy shifts at surfaces and in solids *Surf. Sci. Rep.* **6** 253–415

[39] Mcintyre N S and Cook M G 1975 X-ray photoelectron studies on some oxides and hydroxides of cobalt, nickel, and copper *Anal. Chem.* **47** 2208–13

[40] Spanjaard D, Guillot C, Desjonqueres M-C, Treglia G and Lecante J 1985 Surface core level spectroscopy of transition metals: a new tool for the determination of their surface structure *Surf. Sci. Rep.* **5** 1–85

[41] Subedi A, Yang D, Yun Y, Xu X and Dowben P A 2022 Surface-to-bulk core level shift in $CoFe_2O_4$ thin films *J. Vac. Sci. Technol.* A **40** 023201

[42] Sontu U B, G N R, Chou F C and M V R R 2018 Temperature dependent and applied field strength dependent magnetic study of cobalt nickel ferrite nano particles: synthesized by an environmentally benign method *J. Magn. Magn. Mater.* **452** 398–406

[43] Dowben P A and Miller A 1990 *Surface Segregation Phenomena* (CRC Press)

[44] McIntyre N S and Zetaruk D G 1977 X-ray photoelectron spectroscopic studies of iron oxides *Anal. Chem.* **49** 1521–9

[45] Cheng J, Lu Y, Qiu K, Yan H, Xu J, Han L, Liu X, Luo J, Kim J K and Luo Y 2015 Hierarchical Core/Shell $NiCo_2O_4$@$NiCo_2O_4$ nanocactus arrays with dual-functionalities for high performance supercapacitors and Li-ion batteries *Sci. Rep.* **5** 12099

[46] Dulli H, Dowben P A, Liou S-H and Plummer E W 2000 Surface segregation and restructuring of CMR manganese perovskites: $la_{0.65}Sr_{0.35}MnO_3$ *Phys. Rev.* B **62** R14629–32

[47] Cheng R, Xu B, Borca C N, Sokolov A, Yang C-S, Yuan L, Liou S-H, Doudin B and Dowben P A 2001 Characterization of the native Cr_2O_3 oxide surface of CrO_2 *Appl. Phys. Lett.* **79** 3122–4

[48] Borca C N, Xu B, Komesu T, Jeong H-K, Liu M T, Liou S-H, Stadler S, Idzerda Y and Dowben P A 2001 Electronic structure modifications induced by surface segregation in $La_{0.65}Pb_{0.35}MnO_3$ *Europhys. Lett.* **56** 722–8